

Compressive Imaging of Subwavelength Structures II. Periodic Rough Surfaces

Albert C. Fannjiang* and Hsiao-Chieh Tseng

*Department of Mathematics, University of California, Davis,
One Shields Ave., University of California, Davis, CA 95616-8633, USA*

**Corresponding author: fannjiang@math.ucdavis.edu*

A compressed sensing scheme for near-field imaging of corrugations of relative sparse Fourier components is proposed. The scheme employs random sparse measurement of near field to recover the angular spectrum of the scattered field. It is shown heuristically and numerically that under the Rayleigh hypothesis the angular spectrum is compressible and amenable to compressed sensing techniques.

Iteration schemes are developed for recovering the surface profile from the angular spectrum. The proposed nonlinear least squares in the Fourier basis produces accurate reconstructions even when the Rayleigh hypothesis is known to be false.

© 2022 Optical Society of America

1. Introduction

Rough surface scattering is of fundamental interest in optics, radiowave propagation and acoustics [4, 5, 28] and forms the basis of near-field imaging which is the operation principle behind such instruments as scanning near-field optical microscopy [3, 16, 20, 25] and near field acoustic microscopy [19]. Near-field imaging is a microscopic technique that breaks the diffraction limit by exploiting the properties of evanescent waves. The signal is collected by placing the detector in a distance much smaller than wavelength λ to the specimen surface. An image of the surface is obtained by mechanically moving the probe in a raster scan of the specimen, line by line, and recording the probe-surface interaction as a function of position. This leads to long scan times for large sample areas or high resolution imaging.

Typically near-field imaging is analyzed by assuming a continuum or dense set of data points [15, 24, 27]. In the present work, we focus on the setting of *sparse, discrete* measurement of near-field from the perspective of compressed sensing theory. This is an extension of the work [14] on potential scattering to the case of rough surface scattering. Surface scattering involves the geometry (i.e. topography) of scatterers and is technically more challenging to deal with than potential scattering.

Consider the scattering problem for a corrugation profile described by the function $z = h(x)$. For simplicity of presentation, we will focus on the case of two-dimensional scalar wave with the Dirichlet boundary condition. The total field u^{tot} satisfies

$$\Delta u^{\text{tot}} + k^2 u^{\text{tot}} = 0 \quad \text{in } \Omega \subset \mathbb{R}^2, \quad k > 0 \quad (1)$$

$$u^{\text{tot}} = 0 \quad \text{on } \partial\Omega, \quad (2)$$

where

$$\Omega = \{\mathbf{r} = (x, z) \in \mathbb{R}^2 : z > h(x)\}, \quad h \in C(\mathbb{R}) \cap L^\infty(\mathbb{R}). \quad (3)$$

The total field models the sound pressure wave or electromagnetic waves in the TE-mode. The Dirichlet boundary condition corresponds to the sound-soft boundary condition in acoustics and in electromagnetism the perfectly conducting boundary condition. Our approach can be easily extended to the three dimensional case as well as to the Neumann boundary condition, corresponding to acoustically hard obstacles, and the Robin boundary condition.

As usual in scattering problem, we write $u^{\text{tot}} = u^{\text{inc}} + u$ where both the scattered wave u and the incident wave u^{inc} satisfy the Helmholtz equation. The Dirichlet condition becomes $u = -u^{\text{inc}}$ on $\partial\Omega$.

In this paper, we focus on the case of periodic surfaces which include diffraction gratings, an important class of optical elements. We assume that h has period L and u^{inc} is the plane incident wave

$$u^{\text{inc}}(\mathbf{r}) = e^{ik\hat{\mathbf{d}} \cdot \mathbf{r}} = e^{ik(x \cos \theta - z \sin \theta)}, \quad \hat{\mathbf{d}} = (\cos \theta, -\sin \theta), \quad 0 < \theta < \pi. \quad (4)$$

Observe that on the boundary $z = h(x)$

$$u(x + L, h(x)) = -e^{ik((x+L) \cos \theta - h(x) \sin \theta)} = e^{ikL \cos \theta} u(x, h(x)). \quad (5)$$

Hence we look for the $(L, k \cos \theta)$ -quasi-periodic (or Floquet periodic) solution satisfying

$$u(x + nL, z) = e^{inLk \cos \theta} u(x, z) \quad \text{for all } (x, z) \in \Omega, \quad n \in \mathbb{Z}. \quad (6)$$

In particular, if $\theta = \pi/2$, then u is L -periodic. To fix the idea, we set $L = 2\pi$.

2. Radiation condition and Rayleigh hypothesis

The existence and uniqueness can be proved under the quasi-periodicity and the radiation conditions on the solution u [18]. The well-posedness for general nonperiodic rough surfaces is given in [1]. Below we discuss the Fourier representation of the scattered field and the associated Rayleigh hypothesis.

For $x \in [-\pi, \pi)$, $z > \sup h \triangleq h_{\max}$, we write the scattered field as the Fourier series

$$u(x, z) = \sum_{n \in \mathbb{Z}} u_n(z) e^{i(n+k \cos \theta)x} = \sum_{n \in \mathbb{Z}} u_n(z) e^{ik\alpha_n x} \quad (7)$$

with

$$\alpha_n = \frac{n}{k} + \cos \theta \quad (8)$$

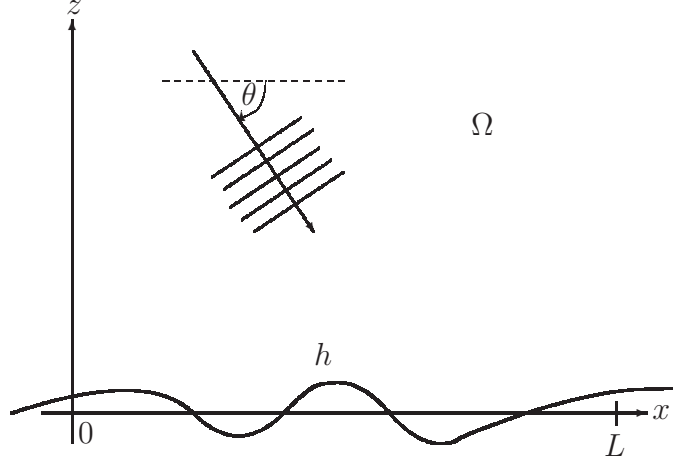


Fig. 1. Surface topography.

where u_n satisfies

$$\ddot{u}_n + k^2(1 - \alpha_n^2)u_n = 0. \quad (9)$$

Solving Eq.(9) and imposing the boundedness of u_n at $z = \infty$ we obtain the general solution as

$$\begin{aligned} u(x, z) = & \sum_{|\alpha_n| \leq 1} a_n e^{ik(\alpha_n x - \beta_n z)} \quad (\text{incoming waves}) \\ & + \sum_{|\alpha_n| \leq 1} b_n e^{ik(\alpha_n x + \beta_n z)} \quad (\text{outgoing waves}) \\ & + \sum_{|\alpha_n| > 1} c_n e^{ik(\alpha_n x + \beta_n z)} \quad (\text{evanescent waves}) \end{aligned} \quad (10)$$

where β_n is given by

$$\beta_n = \begin{cases} \sqrt{1 - \alpha_n^2}, & |\alpha_n| \leq 1 \\ i\sqrt{\alpha_n^2 - 1}, & |\alpha_n| > 1. \end{cases} \quad (11)$$

The *Rayleigh radiation condition* for the region above the grooves $z > h_{\max}$ amounts to dropping the incoming waves in Eq.(10):

$$u(x, z) = \sum_{n \in \mathbb{Z}} u_n e^{ik(\alpha_n x + \beta_n z)}, \quad z > h_{\max}. \quad (12)$$

However, in the region inside the grooves $z < h_{\max}$ multiple scattering may occur and Eq.(12) may not represent the true scattered wave in this region. For shallow corrugations, Eq.(12) should hold in the grooves and this is the Rayleigh hypothesis. For instance, the Rayleigh hypothesis holds for the sinusoidal profile $h(x) = b \sin(ax)$ with $|ab| < 0.448$ [22, 23, 28]. On the other hand, for a general periodic surface the validity of the Rayleigh hypothesis may be difficult to assess [17]. The failure of the Rayleigh hypothesis Eq.(12) manifests in the breaking down of the analytic continuation of Eq.(12) inside grooves.

3. Inverse scattering formulation

Inverse scattering seeks to reconstruct $h(x)$ by transmitting incident wave u^{inc} and measuring the scattered field u at certain locations. Moreover, in order to resolve subwavelength structure which is hidden in the evanescent waves the measurement should be carried out in the near-field.

Due to the quasi-periodicity, we may consider the scattered field u in the union of

$$\Omega_\Gamma \triangleq \{(x, z) \in \Omega, x \in [-\pi, \pi)\} \quad (13)$$

and

$$\Gamma \triangleq \{(x, z) \in \partial\Omega: x \in [-\pi, \pi)\}. \quad (14)$$

For $z > h(x)$ we have the outgoing scattered wave representation Eq.(12) with [2]

$$u_n = \frac{i}{4\pi k \beta_n} \int_{-\pi}^{\pi} e^{-ik(\alpha_n x' + \beta_n h(x'))} \left(-\frac{\partial u^{\text{tot}}(\mathbf{r}')}{\partial \nu'} \Big|_{\mathbf{r}' \in \Gamma} \right) \sqrt{1 + \dot{h}^2(x')} dx'. \quad (15)$$

To ensure $\beta_n \neq 0$ in Eq.(15), we assume that $|\alpha_n| \neq 1$, i.e.,

$$\left| \cos \theta + \frac{n}{k} \right| \neq 1, \quad n \in \mathbb{Z} \quad (16)$$

to avoid all grazing modes. In the case of normal incidence $\theta = \pi/2$, Eq.(16) means that the wavenumber k is not an integer.

A key assumption for our approach is that h has a *small number* of significant Fourier coefficients, namely the Fourier coefficients are sparse or compressible. Writing $h(x) = \sum_{n \in \mathbb{Z}} \hat{h}_n e^{inx}$, we say that $\hat{\mathbf{h}} = \{\hat{h}_n\}$ is s -sparse if $\|\hat{\mathbf{h}}\|_0$, the number of nonzero elements of $\hat{\mathbf{h}}$, is less or equal to a small integer s . Note that $\hat{h}_{-n}^* = \hat{h}_n$ since h is real-valued. Without loss of generality, we assume that $\hat{h}_0 = 0$.

For reconstruction of $h(x)$ we utilize the sparsity of $\hat{\mathbf{h}}$ which surprisingly yields compressibility of the scattering amplitude u_n . Compressive sensing techniques can then used to effectively recover those modes.

Let (x_j, z_0) , $j = 1, 2, \dots, m$, be the sensor locations for measuring the scattered field where $z_0 > h_{\max}$ is fixed and x_j are randomly and independently chosen from $[-\pi, \pi)$ according to the uniform distribution.

In view of the identify

$$u(x_j, z_0) e^{-ik \cos \theta x_j} = \sum_{n \in \mathbb{Z}} e^{inx_j} u_n e^{ik \beta_n z_0} \quad (17)$$

from Eq.(12), let us consider the following inverse problem $Y = \mathbf{A}X$, with entries

$$X_n = u_n e^{ik \beta_n z_0} \sqrt{m} \quad (18)$$

$$Y_j = u(x_j, z_0) e^{-ik x_j \cos \theta} \quad (19)$$

$$\mathbf{A} = [A_{j,n}] = \frac{1}{\sqrt{m}} e^{inx_j} \quad (20)$$

where n is restricted to a finite, but sufficiently large interval ranged from $-N/2$ to $N/2 - 1$. In general the system Eq.(18)-Eq.(20) is highly underdetermined for any $m < \infty$.

Surprisingly, sparse Fourier coefficients $\{\hat{h}_n\}$ give rise to sparse or compressible $\{u_n\}$ and therefore X which can be reconstructed by compressed sensing.

4. Compressive sensing (CS)

The main thrust of compressed sensing [7, 13] is to convert the noisy underdetermined system

$$Y = \mathbf{A}X + E \quad (21)$$

into the L^1 -based optimization problem

$$\min \|X\|_1 \quad \text{subject to} \quad \|Y - \mathbf{A}X\|_2 \leq \epsilon \triangleq \|E\|_2 \quad (22)$$

where E is the external noise vector. Eq.(22) is called the Basis Pursuit (BP) [8]. In addition to quadratic programming, many iterative and greedy algorithms are available for solving the system Eq.(21).

Let us first review a basic notion in CS which provides a performance guarantee for BP. We say a matrix $\mathbf{A} \in \mathbb{C}^{m \times N}$ satisfies the restricted isometry property (RIP) if

$$(1 - \delta) \|Z\|_2^2 \leq \|\mathbf{A}Z\|_2^2 \leq (1 + \delta) \|Z\|_2^2, \quad \delta \in (0, 1) \quad (23)$$

holds for all s -sparse $Z \in \mathbb{C}^N$. The smallest constant satisfying Eq.(23) is called the restricted isometry constant (RIC) of order s and denoted by δ_s .

The following theorem says that the random Fourier matrix satisfies RIP if m is sufficiently large.

Theorem. [26] Let $\xi_j \in [0, 1]$, $j = 1, 2, \dots, m$ be independent uniform random variables. If

$$\frac{m}{\ln m} \geq C\delta^{-2}s \ln^2 s \ln N \ln \frac{1}{\eta}, \quad \eta \in (0, 1) \quad (24)$$

for some universal constant C and sparsity level s , then the restricted isometry constant of the random Fourier measurement matrix with

$$A_{nj} = \frac{1}{\sqrt{m}} e^{2\pi i n \xi_j}, n = -N/2, \dots, N/2 - 1, \quad (25)$$

satisfies $\delta_s \leq \delta$ with probability at least $1 - \eta$.

Denote X_s to be the best s -term approximation of the solution X , and let \tilde{X} be the solution of BP Eq.(22).

Theorem. [6] Let \mathbf{A} satisfy the RIP with

$$\delta_{2s} < \sqrt{2} - 1 \quad (26)$$

and \tilde{X} be the solution to BP. Then

$$\|\tilde{X} - X\|_2 \leq C_0 \frac{1}{\sqrt{s}} \|X_s - X\|_1 + C_1 \epsilon, \quad \|\tilde{X} - X\|_1 \leq C_0 \|X_s - X\|_1 + C_1 \epsilon \quad (27)$$

for some constants C_0, C_1 independent of X .

Once the estimate \tilde{X} is obtained from BP, we reconstruct u_n by

$$\tilde{u}_n = \frac{1}{\sqrt{m}} e^{-ik\beta_n z_0} \tilde{X}_n. \quad (28)$$

The problem with Eq.(28) is that the evanescent modes yield exponentially large factor $e^{-ik\beta_n z_0}$ for

$$|\alpha_n| = \left| \cos \theta + \frac{n}{k} \right| > 1. \quad (29)$$

For n sufficiently large, this can magnify the error in \tilde{X}_n and produce undesirable result in \tilde{u}_n . This observation also shows that X may be much more compressible than $\{u_n\}$.

A simple remedy would be to apply the hard thresholding by restricting the identity Eq.(28) up to n_0 sufficiently small and setting the rest of \tilde{u}_n zero for $|n| > n_0$. Let us now give a rough estimate for the number of modes that should be preserved by the hard thresholding rule.

We define the stably recoverable evanescent modes to be those modes satisfying Eq.(29) and

$$k |\beta_n| z_0 \leq C_e \quad (30)$$

for some constant C_e (in [14], $C_e = 2\pi$). On the other hand,

$$\beta_n = \sqrt{\cos^2 \theta + 2 \frac{n}{k} \cos \theta + \frac{n^2}{k^2} - 1} \geq \frac{|n|}{k} - 1. \quad (31)$$

Hence the stably recoverable modes necessarily satisfy

$$k \left(\frac{|n|}{k} - 1 \right) z_0 \leq k |\beta_n| z_0 \leq C_e \quad (32)$$

or equivalently

$$|n| \leq n_0 \triangleq \frac{C_e}{z_0} + k \quad (33)$$

which is a rough characterization of the stably recoverable (evanescent) modes. We see that n_0 increases as k increases or z_0 small.

Summing up the previous analysis we conclude the recoverability of the scattering amplitude $\{u_n\}$ by the following theorem:

Theorem. Let $z_0 > h_{\max}$ be fixed and let x_j , $j = 1, 2, \dots, m$ be i.i.d uniform random variables in $[-\pi, \pi)$. Let $n_0 = \frac{C_e}{z_0} + k$ for some positive constant $C_e > 0$. Let \tilde{X} , X_s be the BP solution and the best s -term approximated solution of the system Eq.(21) respectively, and assume

$$\frac{m}{\ln m} \geq C \frac{1}{\delta^2} s \ln^2 s \ln N \ln \frac{1}{\eta} \quad (34)$$

for some universal constant C and $\eta \in (0, 1)$. Let $\mathbf{u} = (u_{-n_0}, \dots, u_{n_0})$, $\tilde{\mathbf{u}} = (u_{-n_0}, \dots, u_{n_0})$ where $u_{\tilde{n}}$ is given by Eq.(28). Then one can reconstruct the solution $\tilde{\mathbf{u}}$ with

$$\|\tilde{\mathbf{u}} - \mathbf{u}\|_2 \leq \frac{e^{C_e}}{\sqrt{m}} \left(C_0 \frac{1}{\sqrt{s}} \|X_s - X\|_1 + C_1 \epsilon \right) \quad (35)$$

for some constants C_0, C_1 with probability at least $1 - \eta$.

Proof. Without loss of generality, we prove for the case that x_j , $j = 1, 2, \dots, m$, are i.i.d uniform random variables in $[0, 2\pi)$, and consequently the matrix A , defined in Eq.(21), is the random Fourier measurement Eq.(25) where ξ_j are i.i.d uniform random variables in $[0, 1)$. It is equivalent to the case where x_j are i.i.d uniform random variables in $[-\pi, \pi)$: One can write $x_j = 2\pi(\xi_j - \frac{1}{2})$ and the sensing matrix A is then

$$[A_{j,n}] = \frac{1}{\sqrt{m}} e^{in2\pi(\xi_j - \frac{1}{2})} = \frac{1}{\sqrt{m}} e^{2\pi in \xi_j} (-1)^n. \quad (36)$$

By combining the factor $(-1)^n$ into X_n and writing $W_n = (-1)^n X_n$, $n = -N/2, \dots, N/2 - 1$, we have $\|\tilde{W} - W\|_2 = \|\tilde{X} - X\|_2$, $\|W_s - W\|_1 = \|X_s - X\|_1$, where \tilde{W} and W_s are defined in the same manner.

Under the assumption of the matrix A , we have the estimate

$$\|\tilde{X} - X\|_2 \leq C_0 \frac{1}{\sqrt{s}} \|X_s - X\|_1 + C_1 \epsilon \quad (37)$$

for a desired sparsity level s for some constants C_0, C_1 with probability at least $1 - \eta$. On the other hand,

$$\|\tilde{X} - X\|_2^2 = \sum_{n=-n_0}^{n_0} |\tilde{u}_n e^{ik\beta_n z_0} \sqrt{m} - u_n e^{ik\beta_n z_0} \sqrt{m}|^2 + \sum_{n \in \Lambda} |\tilde{X}_n - X_n|^2 \quad (38)$$

where $\Lambda \triangleq \{-N/2, \dots, -n_0 + 1, n_0 + 1, N/2 - 1\}$. Moreover, for $|n| \leq n_0$ we have $0 < |e^{-C_e}| \leq |e^{ik\beta_n z_0}| \leq 1$, which gives

$$\|\tilde{X} - X\|_2^2 \geq m |e^{-C_e}|^2 \sum_{n=-n_0}^{n_0} |\tilde{u}_n - u_n|^2 + 0 = \frac{m}{e^{2C_e}} \|\tilde{\mathbf{u}} - \mathbf{u}\|_2^2 \quad (39)$$

where $\mathbf{u} = (u_{-n_0}, \dots, u_{n_0})$ and $\tilde{\mathbf{u}} = (u_{-n_0}, \dots, u_{n_0})$. Combining these inequalities, we have the estimate that one can reconstruct $\tilde{\mathbf{u}}$ with

$$\|\tilde{\mathbf{u}} - \mathbf{u}\|_2 \leq \frac{e^{C_e}}{\sqrt{m}} \left(C_0 \frac{1}{\sqrt{s}} \|X_s - X\|_1 + C_1 \epsilon \right). \quad (40)$$

for some constants C_0, C_1 with probability at least $1 - \eta$.

□

5. Compressibility of the angular spectrum

Let us now analyze the compressibility of coefficients $\{u_n\}$. We present a heuristic argument suggesting that the angular spectrum of the scattered field is sparse for shallow corrugations.

Assuming the validity of the Rayleigh Hypothesis we have

$$-u^{\text{inc}}(x, h(x)) = u(x, h(x)) = \sum_{n \in \mathbb{Z}} u_n e^{ik(\alpha_n x + \beta_n h(x))}, \quad (41)$$

or equivalently

$$-e^{-ikh(x) \sin \theta} = \sum_{n \in \mathbb{Z}} u_n e^{ik\beta_n h(x)} e^{inz}. \quad (42)$$

For sufficiently flat and smooth surface h the nearly normal incidence $\theta \approx \frac{\pi}{2}$ tends to produce nearly specular diffracted wave [27] and hence $\{u_n\}$ is concentrated at $n = 0$. This observation suggests that it may be reasonable to approximate the outgoing wavevector $k\beta_n$ by the negative incoming wavevector $k\beta_0$, or equivalently, to replace β_n by $\beta_0 = \sin \theta$. With this approximation, we have

$$\sum_{n \in \mathbb{Z}} u_n e^{inz} \approx \frac{-e^{-ikh(x) \sin(\theta)}}{e^{ik\beta_0 h(x)}} = -1 + 2ikh(x)\beta_0 + \mathcal{O}(k^2|h|^2), \quad (43)$$

provided that the depth of the corrugation is small compared to the wavelength. Hence, we have

$$u_n \approx v_n \triangleq \begin{cases} -1 & n = 0 \\ 2ik\hat{h}_n\beta_0 & n \neq 0 \end{cases} \quad (44)$$

which is sparse by the sparseness assumption on $\{\hat{h}_n\}$. Let $W = \sqrt{m}(v_n e^{ik\beta_n z_0})$. In view of Eq.(18) we have the estimate

$$\|X - X_s\|_1 \approx \|X - W\|_1 = \sum_{n=-N/2}^{N/2-1} \sqrt{m} |e^{ik\beta_n z_0}| |u_n - v_n| \leq \sqrt{m}\epsilon_u \quad (45)$$

where $\epsilon_u \triangleq \sum_{n=-N/2}^{N/2-1} |u_n - v_n|$. The subsequent numerical simulation shows that u_n and v_n given in Eq.(44) are indeed close to each other when the Rayleigh hypothesis is valid.

6. Numerical simulation

6.A. Data synthesis

We compute the scattered field $u(x, z_0)$ by the boundary integral method [11, 21]. The scattered wave can be represented by the Brakhage-Werner type ansatz, i.e. the representation via mixed single-layer (S) and double-layer (K) potentials

$$u = (K - i\eta S)\varphi \quad \text{on } \Omega_\Gamma \quad (46)$$

with a mixed layer density ψ for a constant $\eta > 0$ which can be adjusted to improve the condition number of the system. Explicitly, we can write

$$u(x, z) = \int_{-\pi}^{\pi} \left(\frac{\partial}{\partial \nu'} \Phi((x, z), (x, h(x'))) - i\eta \Phi((x, z), (x, h(x'))) \right) \psi(x') \cdot \sqrt{1 + \dot{h}^2(x')} dx'. \quad (47)$$

Taking the limit $z \rightarrow h(x)^+$ and using the properties of single and double layer potentials, we obtain the boundary integral equation [9, 11]

$$-u^{\text{inc}}(x, h(x)) = \frac{1}{2}\psi(x) + \int_{-\pi}^{\pi} \left(\frac{\partial}{\partial \nu'} \Phi((x, h(x)), (x', h(x'))) - i\eta \Phi((x, h(x)), (x', h(x'))) \right) \psi(x') \sqrt{1 + \dot{h}^2(x')} dx' \quad (48)$$

(see Appendix). Note that the integral in Eq.(48) has weakly singular kernel, and the integral exists as an improper integral since the periodic Green's function

$$\Phi(\mathbf{r}, \mathbf{r}') = \frac{i}{4} \sum_{n \in \mathbb{Z}} e^{2\pi i n k \cos \theta} H_0^{(1)}(k |\mathbf{r} - \mathbf{r}' - 2\pi n(1, 0)|), \quad x, x' \in [-\pi, \pi) \quad (49)$$

has the same singularity as $H_0^{(1)}(x) \approx 1 + \frac{2i}{\pi}(\ln \frac{x}{2} + \gamma)$ where $\gamma \approx 0.5772$ is the Euler-Mascheroni constant. Moreover,

$$\frac{\partial}{\partial \nu'} H_0^{(1)}(k |\mathbf{r} - \mathbf{r}'|) = -k H_1^{(1)}(k |\mathbf{r} - \mathbf{r}'|) \frac{(\mathbf{r} - \mathbf{r}') \cdot \nu(\mathbf{r}')}{|\mathbf{r} - \mathbf{r}'|} \quad (50)$$

converges to a finite limit (a curvature-like term w.r.t. the boundary) as $\mathbf{r} \rightarrow \mathbf{r}'$ [10] implying the boundedness of $\frac{\partial}{\partial \nu'} \Phi$ on Γ .

With ψ solved from Eq.(48) and the Sommerfeld integral representation

$$H_0^{(1)}(k |\mathbf{r}|) = \frac{1}{\pi} \int e^{ik(|z| + \beta x \alpha)} \frac{d\alpha}{\beta}, \quad (51)$$

where

$$\beta = \begin{cases} \sqrt{1 - \alpha^2}, & |\alpha| < 1 \\ i\sqrt{\alpha^2 - 1}, & |\alpha| > 1 \end{cases} \quad (52)$$

we obtain from Eq.(47) the outgoing wave expansion for the scattered field

$$u(x, z) = \sum_{n \in \mathbb{Z}} e^{ik(\alpha_n x + \beta_n z)} \left(\frac{1}{4\pi} \int_{-\pi}^{\pi} e^{-ik(\alpha_n x' + \beta_n h(x'))} g_n(x') \psi(x') dx' \right), \quad z > h_{\max} \quad (53)$$

with

$$g_n(x') = k - k\dot{h}(x') \frac{\alpha_n}{\beta_n} + \frac{\eta}{\beta_n} \sqrt{1 + \dot{h}^2(x')}. \quad (54)$$

Comparing Eq.(53) with Eq.(12) we arrive at the expression

$$u_n = \frac{1}{4\pi} \int_{-\pi}^{\pi} e^{-ik(\alpha_n x' + \beta_n h(x'))} g_n(x') \psi(x') dx' \quad (55)$$

relating the angular spectrum of the scattered field to the mixed layer density ψ .

Eq.(48) and Eq.(55) motivates the following iterative reconstruction scheme. Given $h^{(m)}$, $m = 1, 2, 3, \dots$ first solve for $\psi^{(m)}$ from

$$\begin{aligned} -u^{\text{inc}}(x, h^{(m)}(x)) &= \frac{1}{2} \psi^{(m)}(x) + \int_{-\pi}^{\pi} \left(\frac{\partial}{\partial \nu'} \Phi((x, h^{(m)}(x)), (x', h^{(m)}(x'))) \right. \\ &\quad \left. - i\eta \Phi((x, h^{(m)}(x)), (x', h^{(m)}(x'))) \right) \psi^{(m)}(x') \sqrt{1 + |\dot{h}^{(m)}|^2(x')} dx' \end{aligned} \quad (56)$$

and then solve for $h^{(m+1)}$ from

$$u_n = \frac{1}{4\pi} \int_{-\pi}^{\pi} e^{-ik(\alpha_n x' + \beta_n h^{(m)}(x'))} g_n^{(m+1)}(x') \psi^{(m)}(x') dx', \quad n \in \mathbb{Z} \quad (57)$$

$$g_n^{(m+1)}(x') = k - k \dot{h}^{(m+1)}(x') \frac{\alpha_n}{\beta_n} + \frac{\eta}{\beta_n} \sqrt{1 + |\dot{h}^{(m)}|^2(x')}. \quad (58)$$

Note that both Eq.(56) and Eq.(57) are linear equations.

A natural candidate for the initial guess of the above iteration is the one obtained under the Rayleigh hypothesis that the validity of Eq.(53) is extended to the region $z > h(x)$. Specifically, we extend Eq.(53) all the way to boundary and study the nonlinear equation Eq.(41). Indeed, this alone produces excellent results for shallow corrugations and will be the focus of the following numerical experiments. Scattering and imaging of shallow corrugations can also be treated by assuming the Born approximation [12].

In our numerical simulations, we set 128 nodes to solve the boundary integral equation Eq.(48) by the Nyström method, with $\eta = 1$. Figure 2 shows two examples of the computed scattered field. We define $R_a(h) \triangleq \max_n 2|n\hat{h}_n|$ for a rough metric of the validity of the Rayleigh hypothesis.

6.B. Surface reconstruction

Solve for $h(x)$ from Eq.(41), we consider the following three algorithms: the first two are pointwise matching schemes and the third is a global fitting scheme.

1. Point-wise, fixed-point iteration for $h(x)$, $\forall x \in [-\pi, \pi)$. A fixed point iteration algorithm was introduced in [15, 27] and is described below. The initial condition $h^{[0]}(x)$ is chosen in the following way. For $\theta \approx \frac{\pi}{2}$ the angular spectrum $\{u_n\}$ is concentrated at $n = 0$. Substituting β_n by 1 in Eq.(41) yields

$$e^{ikh(x)} \cdot \sum_{n \in \mathbb{Z}} u_n e^{ik\alpha_n x} = -e^{ik(x \cos \theta - h(x) \sin \theta)}. \quad (59)$$

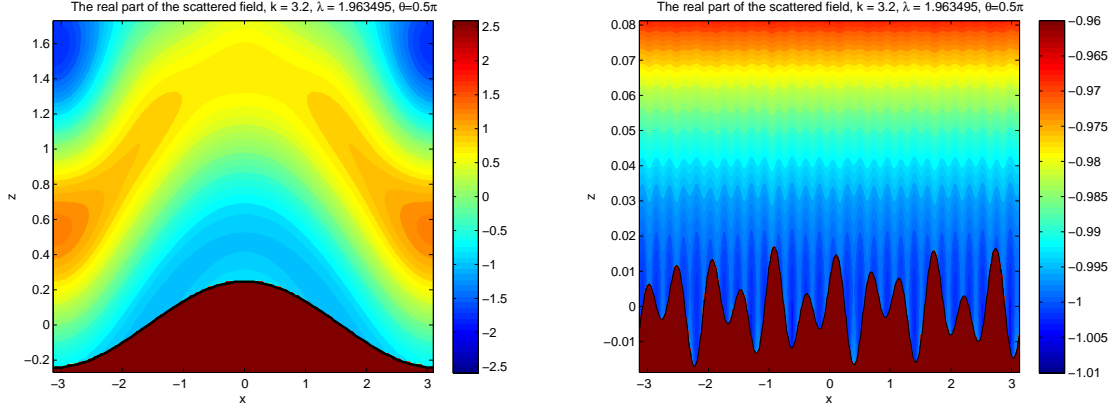


Fig. 2. The real part of the scattered field induced by the profile $h(x) = 0.2454 \sin(x)$ (left) and the profile $h(x) = 0.01 \sin(12x) + 0.007 \cos(7x)$ (right) with $L = 2\pi$ and vertical incident wave.

One solves Eq.(59) by the iterative scheme

$$h^{[0]}(x) = \frac{\ln \left(- \sum_{n \in \mathbb{Z}} u_n e^{ik\alpha_n x} \right)}{-2ik}, \quad (60)$$

$$h^{[n+1]}(x) = \frac{\ln \left(- \sum_{n \in \mathbb{Z}} u_n e^{ik \left(\alpha_n x + (\beta_n - 1) h^{[n]}(x) \right)} \right)}{-2ik} \quad (61)$$

for $n = 1, 2, \dots$ and all $x \in [-\pi, \pi)$.

2. Newton's method. From Eq.(41), for each $x \in [-\pi, \pi)$ we set

$$e(h; x) = e^{ikx_j \cos \theta} e^{-ikh \sin \theta} + \sum_{n \in \mathbb{Z}} u_n e^{ik\alpha_n x_j} e^{ik\beta_n h}, \quad (62)$$

and solve $e(h, x) = 0$ for $h(x)$ by Newton's method

$$h^{[i+1]} = h^{[i]} - \frac{e(h^{[i]}; x)}{\frac{d}{dh} e(h^{[i]}; x)} \quad (63)$$

with initial value Eq.(60).

3. Nonlinear least squares fitting. Let

$$F(\mathbf{a}) = \left\| e \left(\sum_n a_n \phi_n(\cdot), \cdot \right) \right\|^2 = \sum_j \left| e \left(\sum_n a_n \phi_n(x_j), x_j \right) \right|^2, \quad (64)$$

where $e(h; x_j)$ is defined in Eq.(62) and $\mathbf{a} = (a_1, a_2, \dots)$ is the vector of the coefficients of an expansion of h corresponding to a frame $\{\phi_n\}$, i.e., $h = \sum_n a_n \phi_n$. Consider

minimizing the nonlinear least square

$$\min_{\mathbf{a}} F(\mathbf{a}). \quad (65)$$

The basis function are chosen to be $\sin(nx)$ and $\cos(nx)$ for $n \in \Pi \subset \mathbb{N}$, where the index set Π contains those indices n such that $|\tilde{u}_n|$ are relatively large. The Matlab subroutine `lsqnonlin` is applied, which is based on the subspace trust region method.

6.C. Examples

In the following examples we apply vertical incident wave, $\theta = \frac{\pi}{2}$, with the wave number $k = 3.2$ (i.e., the wavelength $\lambda \approx 1.9635$). After synthesizing $u(x_j, z_0)$ for $j = 1, 2, \dots, m$, 1% additive noise, with respect to $\|u(\cdot, z_0)\|_2/\sqrt{m}$, is added to the measured scattered field u . The profile functions h are $L = 2\pi$ periodic, defined in one period $[-\pi, \pi)$, and periodically extended into \mathbb{R} . The bound for the exponential factor is set to be $C_e = \log(25)$. Yall1 [29] algorithm, a Basis Pursuit solver, is applied to solve Eq.(20) for vector \tilde{X} . To avoid exponential amplification of small components of \tilde{X} , we apply a threshold level $\tau = 10\% \cdot \max_{n \neq 0} |\tilde{X}_n|$ and filter out the components below τ , then compute \tilde{u}_n from Eq.(28).

In Figures 3-8, the right panels show the exact profile $h(x)$ (black solid line), and the reconstruction under the three algorithms: Newton's method "**Newton**", fixed point iteration "**Fixed pt iter**", and nonlinear least squares fitting "**NLS fit**". The length of the black strip on the top of each plot indicates the wavelength, and its height indicates the vertical coordinate z_0 of the sampling points. The left and middle panels show the real (left) and imaginary parts (middle) the angular spectrum u_n (blue crosses), the estimated angular spectrum \tilde{u}_n (red dots), and the theoretical estimate v_n (green circles). Note the different scales for the real and imaginary parts in Figures 3-6 where R_a is relatively small. This is no longer the case in Figures 7 and 8 for which the Rayleigh hypothesis is known to be false.

Figures 3 and 4 show the results for profiles $h(x)$ with sparse Fourier coefficients. The prediction v_n captures well the dominant component $\Re[u_0]$ and so does the sparse reconstruction \tilde{u}_n the other significant components of the angular spectrum. For reconstruction (right panels) the nonlinear least squares is the best performer while the pointwise iterative methods may produce visible undershoots at the peaks and troughs.

For the Gaussian profile (Fig 5) and subwavelength double-peaks (Fig 6), again v_n captures well the dominant component $\Re[u_0]$ and so does the sparse reconstruction \tilde{u}_n most other significant components of the angular spectrum. The angular spectrum for the latter case occupies a wider range of modes than the former case since the two peaks are sharper than the Gaussian. As a consequence, the reconstruction is more accurate in the former case. For the latter case, all three reconstructions undershoot the peaks and produce fluctuations at the flat part of the profile.

Figures 7 and 8 are the results for simple sinusoids when the Rayleigh hypothesis is known to fail ($ab > 0.448$). The failure of the Rayleigh hypothesis manifests in the broadening of the support of the angular spectrum. Furthermore, the imaginary part of the angular spectrum is order of magnitudes larger than those in Figures 3-6. As a result, the angular spectrum $\{u_n\}$ is less compressible and not well recovered by the compressed sensing techniques. In both cases, the simple prediction v_n fails to capture the dominant components of the angular spectrum.

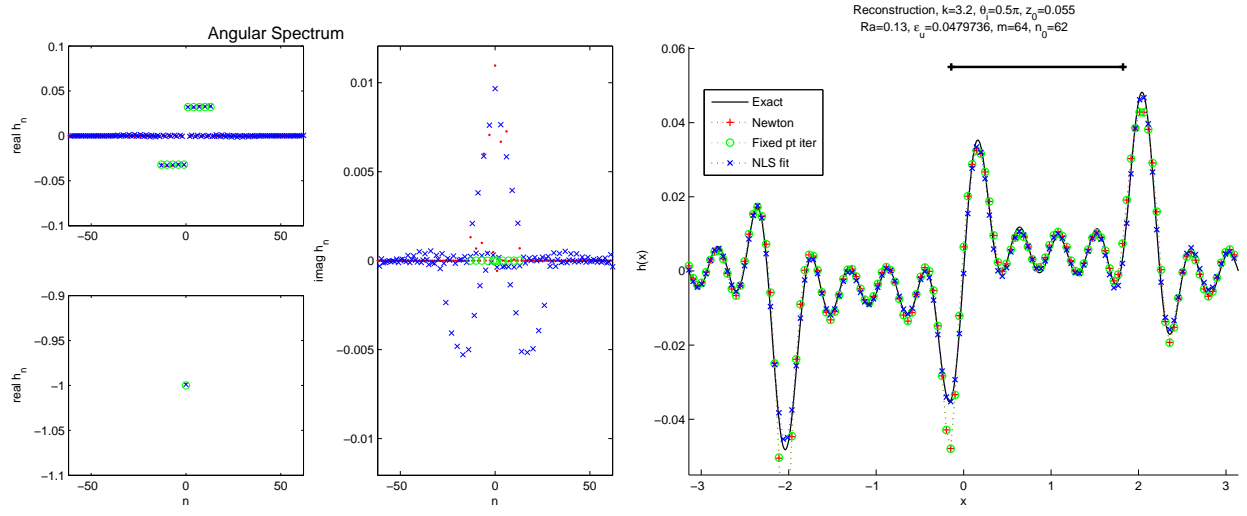


Fig. 3. The profile of 5 Fourier modes $h(x) = 0.01(\sum_{p=0}^4 \sin((1+3p)x))$ and the reconstructions.

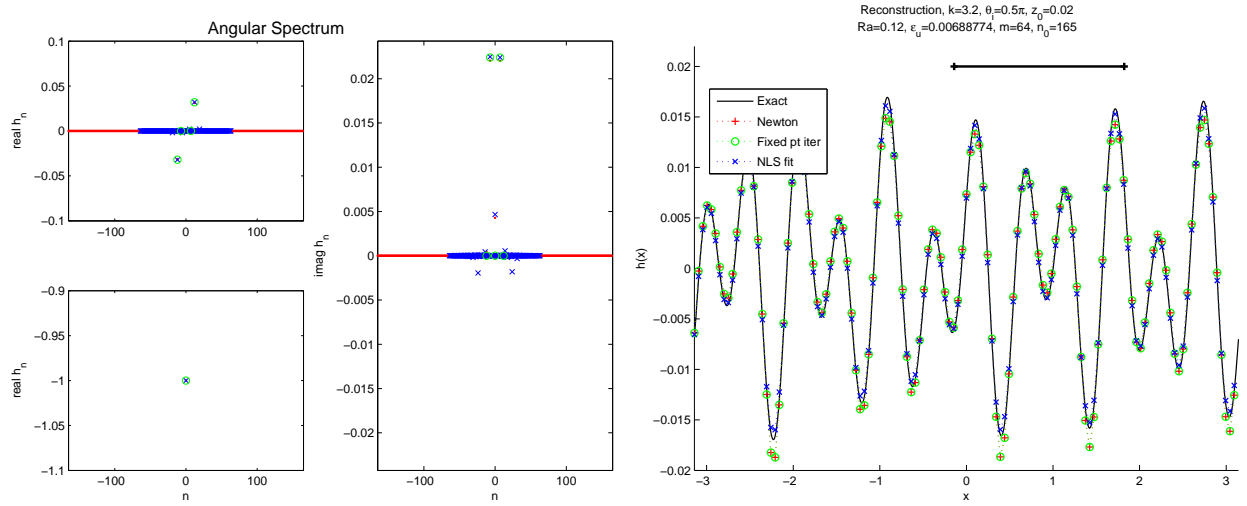


Fig. 4. Profile of two Fourier modes $h(x) = 0.01 \sin(12x) + 0.007 \cos(7x)$ and the reconstructions.

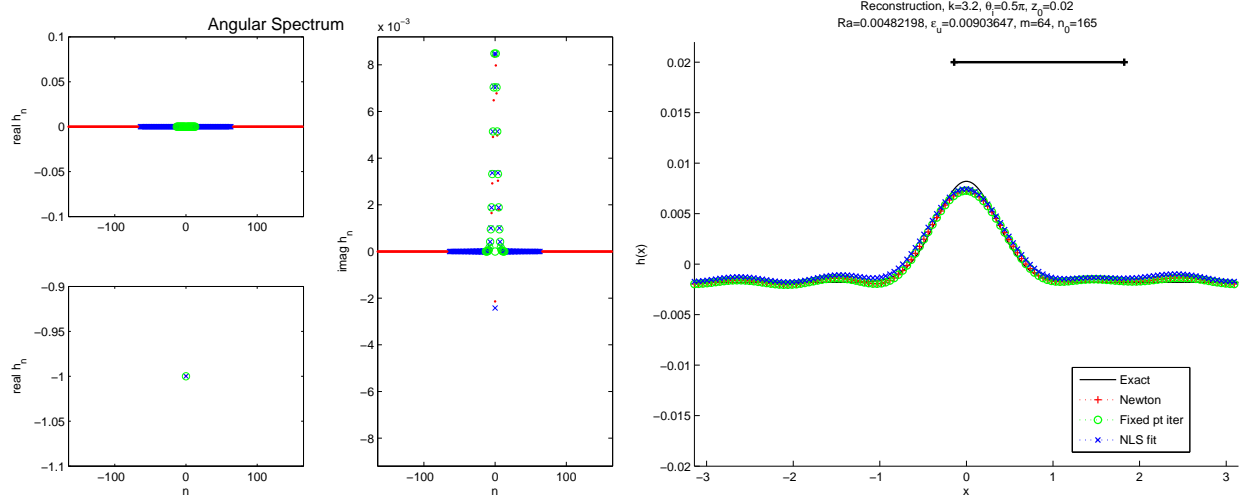


Fig. 5. Periodized Gaussian $h(x) = b(e^{-(ax)^2} - \frac{\text{erf}(a\pi)}{\pi\sqrt{\pi}}) \cdot \tilde{\chi}_{[-0.9\pi, 0.9\pi]}(x)$, $a = 2$, $b = 0.01$ and the reconstructions. Here $\tilde{\chi}$ is a smoothed indicator function.

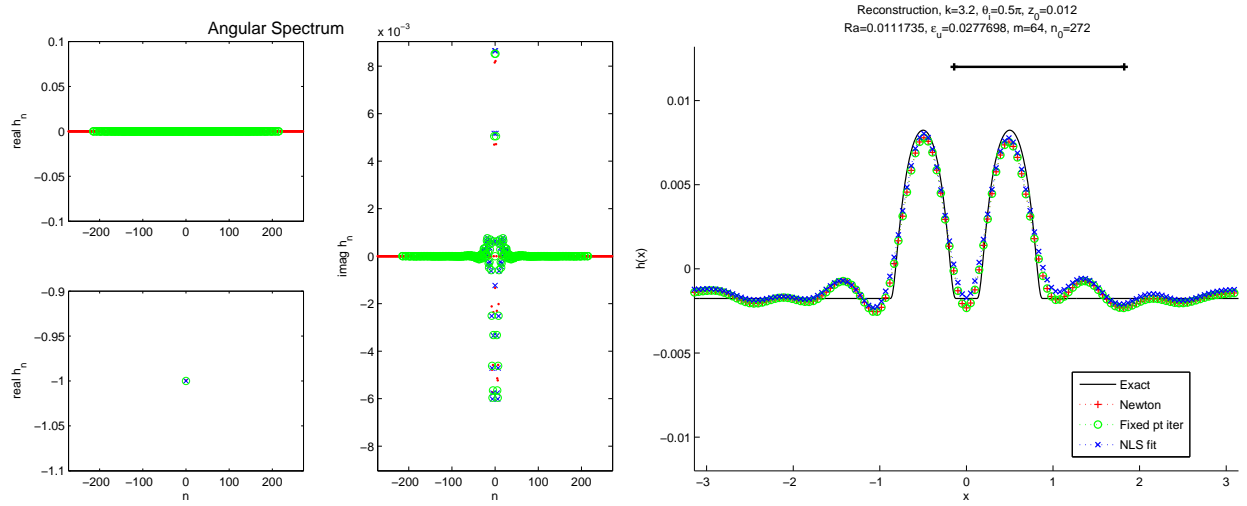


Fig. 6. Double subwavelength peaks $h(x) = b(\zeta(a(x-\frac{1}{2}))+\zeta(a(x+\frac{1}{2})))$, $a = 2.5$, $b = 0.01$, $\zeta(x) = \exp(1 - \frac{1}{x^2-1}) \chi_{(-1,1)}(x) + c_0$ and the reconstructions. Here the constant c_0 is chosen such that $\hat{\zeta}_0 = 0$.

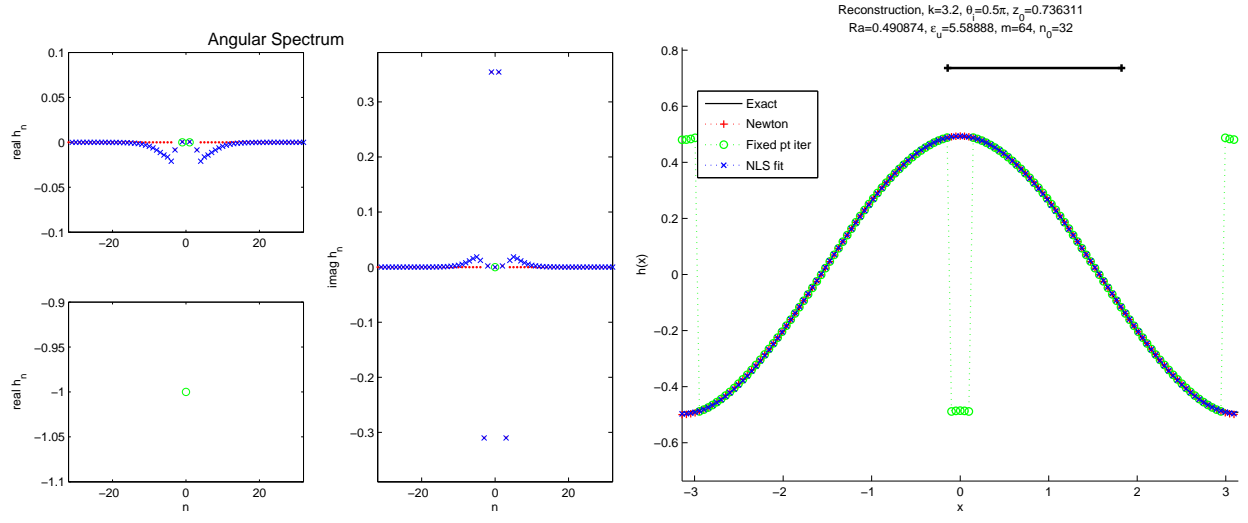


Fig. 7. $h(x) = 0.491 \cos(x)$

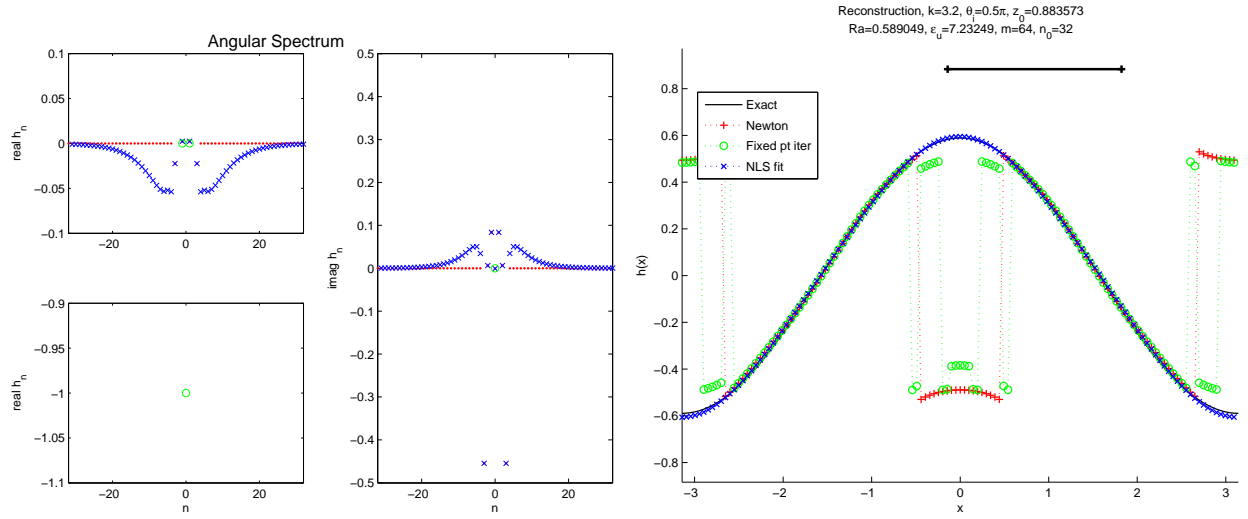


Fig. 8. $h(x) = 0.589 \cos(x)$.

Nevertheless, the nonlinear least squares fitting provides an accurate reconstruction of the profile in both cases. The Newton iteration converges in Figure 7 but fails near the peaks and troughs in Figure 8 while the fixed point iteration fails to converge near the peaks and troughs in both cases. When ab is further increased (to, e.g. 0.736), then all three methods fail to recover the profile.

7. Conclusion

We have proposed a compressed sensing scheme for near-field imaging of corrugations of relative sparse Fourier components. The scheme employs random sparse measurement of near field to recover the angular spectrum of the scattered field. We have shown heuristically and numerically that under the Rayleigh hypothesis the angular spectrum is indeed sparse or compressible and amenable to compressed sensing techniques.

We then develop iteration schemes for recovering the surface profile from the angular spectrum. Specifically, under the Rayleigh hypothesis we have tested three iterative schemes. The nonlinear least squares in the Fourier basis has the best performance among the three and produces accurate reconstructions even when the Rayleigh hypothesis is known to be false.

The full iteration scheme Eq.(56)-Eq.(57) beyond the limitation of the Rayleigh hypothesis will require non-sparse measurements for the angular spectrum data and will be studied elsewhere.

Acknowledgement. The research supported in part by NSF Grant DMS 0908535.

References

1. T. Arens and T. Hohage. "On radiation conditions for rough surface scattering problems." *Journal of Applied Mathematics* **70** (2005), 839-847.
2. T. Arens, S. N. Chandler-Wilde and J. A. DeSanto. "On integral equation and least squares methods for scattering by diffraction gratings." *Communications in Computational Physics* **1** (2006), 1010-1042.
3. E.A. Ash and G. Nicholls "Super-resolution aperture scanning microscope". *Nature* **237**, 510-512 (1972).
4. P. Beckmann. "Scattering of light by rough surfaces." *Prog. Opt.* **6** (1968), 53.
5. F. B. Bass and I.M. Fuks. *Wave Scattering from Statistically Rough Surfaces*. Pergamon Press, Oxford, 1980.
6. E. J. Candès. "The restricted isometry property and its implications for compressed sensing." *Comptes Rendus Mathématique* **346** (2008), 589-592.
7. E. J. Candès and T. Tao, "Near-optimal signal recovery from random projections: Universal encoding strategies," *IEEE Trans. Inform. Theory* **52** (2006), 5406 - 5425.
8. S.S. Chen, D.L. Donoho and M.A. Saunders, "Atomic decomposition by basis pursuit," *SIAM Rev.* **43** (2001), 129-159.
9. D. Colton and R. Kress. *Integral Equation Methods in Scattering Theory*. Wiley 1983.
10. D. Colton and R. Kress. *Inverse Acoustic and Electromagnetic Scattering Theory*, 2nd ed. Springer 1998.

11. J. DeSanto, G. Erdmann, W. Hereman and M. Misra. "Theoretical and computational aspects of scattering from rough surfaces: one-dimensional perfectly reflecting surfaces." *Waves in Random Media* **8** (1998), 385-414.
12. G. Derveaux, G. Papanicolaou, and C. Tsogka, "Resolution and Denoising in Near-Field Imaging." *Inverse Problems* **22** (2006), 1437-1456.
13. D. L. Donoho, "Compressed sensing," *IEEE Trans. Inform. Theory* **52** (2006) 1289-1306.
14. A. Fannjiang. "Compressive imaging of subwavelength structures." *SIAM J. Imag. Sci.* **2** (2009) 1277-1291.
15. N. Garcia and M. Nieto-Vesperinas. "Near-field optics inverse-scattering reconstruction of reflective surfaces." *Optics Letters* **18** (1993), 2090-2092.
16. B. Hecht, B. Sick, U.P. Wild, V. Deckert, R. Zenobi, O.J.F. Martin, and D.W. Pohl. "Scanning near-field optical microscopy with aperture probes: Fundamentals and applications". *J. Chem. Phys.* **112** (18): 7761-7774 (2000).
17. J. B Keller. "Singularities and Rayleigh's hypothesis for diffraction gratings." *J. Opt. Soc. Am. A* **17** (2000), 456-457.
18. A. Kirsch. "Diffraction by periodic structures." *Inverse problems in mathematical physics* **422** (1993), 87-102.
19. B.T. Khuri-Yakub, S. Akamine, B. Hadimioglu, H. Yamada and C.F. Quate, "Near field acoustic microscopy", SPIE Vol. 1556 *Scanning Microscopy Instrumentation* 30-39 (1991).
20. A. Lewis, M. Isaacson, A. Harootunian, and A. Murray, "Development of a 500Å spatial resolution light microscope. I. Light is efficiently transmitted through $\lambda/16$ diameter apertures." *Ultramicroscopy* **13** (3): 227-231 (1984).
21. A. Meier, T. Arens, S. N. Chandler-Wilde and A. Kirsch. "A Nyström method for a class of integral equations on the real line with applications to scattering by diffraction gratings and rough surfaces." *Journal of Integral Equations and Applications* **12** (2000) 281-321.
22. R. F. Millar. "On the Rayleigh assumption in scattering by a periodic surface." *Mathematical Proceedings of the Cambridge Philosophical Society* **65** (1969), 773-791.
23. R. F. Millar. "On the Rayleigh assumption in scattering by a periodic surface II." *Mathematical Proceedings of the Cambridge Philosophical Society* **69** (1971), 217-225.
24. M. Nieto-Vesperinas and N. Garcia. "A detailed study of the scattering of scalar waves from random rough surfaces." *Opt. Acta.* **28** (1981), 1651-1672.
25. D.W. Pohl, W. Denk, and M. Lanz "Optical stethoscopy: Image recording with resolution $\lambda/20$ ". *Appl. Phys. Lett.* **44** (7): 651 (1984).
26. H. Rauhut. "Stability results for random sampling of sparse trigonometric polynomials." *IEEE Transactions on Information Theory* **54** (2008), 5661-5670.
27. K. H. Riederer, N. Garcia and V. Celli. "An effective procedure to determine corrugation functions from atomic beam-diffraction intensities." *Surface Science* **108** (1981), 169-180.
28. J. L. Uretsky. "The scattering of plane waves from periodic surfaces." *Annals of Physics* **33** (1965), 400-427.
29. J. Yang and Y. Zhang. "Alternating direction algorithms for L1 problems in compressive sensing." *CAAM, Rice University* **TR09-37** (2010).

A. Derivation of the boundary integral equation Eq.(48)

The term $\frac{1}{2}\psi(x)$ in Eq.(48) arises due to the jump discontinuity for the double layer potential across the boundary, whereas the single layer potential is continuous. More specifically, let

$$u_S(\mathbf{r}) = \int_{\Gamma} \Phi(\mathbf{r}, \mathbf{r}') \psi_S(\mathbf{r}') dS(\mathbf{r}') \quad (66)$$

$$u_D(\mathbf{r}) = \int_{\Gamma} \frac{\partial}{\partial \nu'} \Phi(\mathbf{r}, \mathbf{r}') \psi_D(\mathbf{r}') dS(\mathbf{r}') \quad (67)$$

be the single and double layer potentials respectively for $\mathbf{r} = (x, z) \in \mathbb{R}^2 \setminus \Gamma$. Furthermore we denote $\mathbf{r}^{\pm} = \mathbf{r}_0 \pm \rho \nu(\mathbf{r}_0)$ for some small $\rho > 0$ and $\mathbf{r}_0 \in \Gamma$ (assuming that the boundary is of class C^2 so the representation of \mathbf{r}^{\pm} is unique for \mathbf{r}^{\pm} near the boundary). Clearly

$$\lim_{\rho \rightarrow 0} u_S(\mathbf{r}^+) = \lim_{\rho \rightarrow 0} u_S(\mathbf{r}^-) = u_S(\mathbf{r}_0). \quad (68)$$

On the other hand, write

$$u_D(\mathbf{r}^+) = \psi_D(\mathbf{r}_0) \int_{\Gamma} \frac{\partial}{\partial \nu'} \Phi_0(\mathbf{r}^+, \mathbf{r}') dS(\mathbf{r}') + v(\mathbf{r}^+) \quad (69)$$

$$u_D(\mathbf{r}^-) = \psi_D(\mathbf{r}_0) \int_{\Gamma} \frac{\partial}{\partial \nu'} \Phi_0(\mathbf{r}^-, \mathbf{r}') dS(\mathbf{r}') + v(\mathbf{r}^-) \quad (70)$$

so that

$$\begin{aligned} v(\mathbf{r}^{\pm}) &= \int_{\Gamma} \frac{\partial}{\partial \nu'} \Phi(\mathbf{r}^{\pm}, \mathbf{r}') (\psi_D(\mathbf{r}') - \psi_D(\mathbf{r}_0)) dS(\mathbf{r}') \\ &\quad + \psi_D(\mathbf{r}_0) \int_{\Gamma} \left(\frac{\partial}{\partial \nu'} \Phi(\mathbf{r}^{\pm}, \mathbf{r}') - \frac{\partial}{\partial \nu'} \Phi_0(\mathbf{r}^{\pm}, \mathbf{r}') \right) dS(\mathbf{r}') \end{aligned} \quad (71)$$

where Φ_0 is the Green's function for Laplace equation. It is easy to see that integral Eq.(71) is continuous in the neighborhood of $\rho = 0$.

The jump condition

$$\lim_{\rho \rightarrow 0} (u_D(\mathbf{r}^+) - u_D(\mathbf{r}^-)) = \psi_D(\mathbf{r}_0) \quad (72)$$

now follows from the calculation

$$\int_{\Gamma} \frac{\partial}{\partial \nu'} \Phi_0(\mathbf{r}^{\pm}, \mathbf{r}') dS(\mathbf{r}') = \frac{1}{2} \int_{\partial B_{\rho}(\mathbf{r}_0)} \frac{\partial}{\partial \nu'} \Phi_0(\mathbf{r}^{\pm}, \mathbf{r}') dS(\mathbf{r}') \quad (73)$$

$$= \frac{1}{4\pi\rho} \int_{\partial B_{\rho}(\mathbf{r}_0)} \pm 1 dS(\mathbf{r}') \longrightarrow \pm \frac{1}{2}, \quad \rho \rightarrow 0 \quad (74)$$

by applying the divergence theorem, integrating over the circle $B_{\rho}(\mathbf{r}_0)$ of radius ρ and shrinking radius ρ to 0.